Academia
Materials Science

10.20935/AcadMatSci8486

Research Article

# Sugarcane bagasse-derived xanthan gum improves polyvinyl alcohol films for food packaging

Maria Rita Meyer Ferraz da Costa[1,2], Enio Nazaré de Oliveira Junior[3], Marali Vilela Dias[4], Fábio Gomes Teixeira[5], Julian Christ[2], Lisbeth Garbrecht Thygesen[2], Anand Ramesh Sanadi[2], Gustavo Henrique Denzin Tonoli[1], Mario Guimarães Junior[6,*]

[1] Department of Forest Science, Federal University of Lavras (UFLA), Lavras, Brazil
[2] Department of Geoscience and Natural Resource Management, University of Copenhagen (KU), Frederiksberg, Denmark
[3] Department of Chemistry, Biotechnology and Bioprocess Engineering, Federal University of Sao Joao del Rei (UFSJ), Ouro Branco, Brazil
[4] Department of Food Science, Federal University of Lavras (UFLA), Lavras, Brazil
[5] Packaging Technology Center, Institute of Food Technology, Campinas, Brazil
[6] Electromechanical Department, Federal Center of Technological Education of Minas Gerais (CEFET—MG), Araxa, Brazil
* Correspondence: mgjunior@cefetmg.br

**Received:** 26 June 2026 | **Accepted:** 17 August 2026 | **Published:** 8 September 2026

## Abstract

**Introduction:** The increasing demand for environmentally responsible packaging materials has intensified the search for renewable alternatives to conventional fossil-based plastics. Among the available options, biodegradable polymers show great potential, although their mechanical performance and barrier properties still require improvement for broader industrial use.

**Materials and methods:** In this study, films based on polyvinyl alcohol (PVA) and xanthan gum (XG), including two xanthan gum variants produced from sugarcane bagasse (XGL1 and XGL2), were prepared by the solvent-casting method and evaluated through mechanical, thermal, morphological, spectroscopic, and water vapor barrier analyses.

**Results:** The incorporation of xanthan gum positively affected film performance, particularly for the PVA/XGL1 formulation. This film showed a 37.9% increase in tensile strength compared with pure PVA, an elongation at break of 270.97%, lower water vapor permeability (0.243 g·mm/m$^2$·h·kPa), and a higher contact angle (80.81°), indicating reduced sensitivity to moisture. Fourier transform infrared spectroscopy (FTIR) results suggested strong intermolecular interactions between PVA and xanthan gum, while Field emission gun scanning electron microscopy (FEG-SEM) analysis revealed homogeneous and compact structures.

**Conclusions:** Although the films remained moderately water-soluble and thermal degradation began near 200 °C, the overall performance obtained demonstrates the potential of the PVA/XGL1 blend for food packaging applications. In addition to improving material properties, the use of xanthan gum produced from sugarcane bagasse provides a productive route for valorizing agro-industrial residues, contributing to the development of sustainable packaging materials with reduced environmental impact.

**Keywords**: biodegradable films; xanthan gum; polyvinyl alcohol; food packaging; agro-industrial residues

## 1. Introduction

Food packaging is one of the sectors most dependent on plastic materials, as they contribute significantly to preserving product quality, ensuring safety, and maintaining integrity throughout transportation, storage, and marketing [1, 2]. Among the most widely used polymers in this sector are polypropylene (PP), polyethylene (PE), and polyvinyl chloride (PVC), valued for their mechanical, thermal, and barrier properties. However, the increasing dependence on these materials highlights critical environmental challenges, such as waste accumulation resulting from improper disposal, low biodegradability, and reliance on fossil resources [3–8]. Global production of petroleum-based plastics reached approximately 430.9 million tons in 2024, with PP and PE together accounting for about 177 million tons, reflecting their significant market share and contribution to waste generation.

This scenario conflicts with key Sustainable Development Goals (SDGs) of the UN 2030 Agenda, particularly SDG 12 (Responsible Consumption and Production), SDG 13 (Climate Action), and SDGs 14 and 15 (Life Below Water and Life on Land), which emphasize waste reduction, pollution mitigation, and the transition to sustainable materials. Therefore, the development of environmentally responsible alternatives to replace or reduce the use of conventional polymers has become urgent.

The search for more sustainable packaging alternatives has intensified interest in renewable biopolymers. Their application in biodegradable packaging is particularly attractive because, beyond providing protection to food products, they can also help preserve quality for longer periods when associated with bioactive agents [1, 9]. Despite these advantages, biodegradable materials face important limitations: lower mechanical resistance, weaker barrier performance, and higher production costs compared with traditional polymers. A notable example is the cost difference between polylactic acid (PLA), which ranges from 2.5 to 4.0 USD/kg, and PP, typically priced at 1.0 to 1.5 USD/kg, making biodegradable packaging up to four times more expensive [10]. This economic barrier hampers large-scale industrial adoption and underscores the need for innovation aligned with SDG 9 (Industry, Innovation, and Infrastructure), which promotes the development of clean and accessible technologies.

In this regard, blending different polymers has become an attractive strategy for tailoring the properties of biodegradable materials. By physically combining two or more polymers, it is possible to obtain materials with improved mechanical resistance, thermal behavior, and barrier characteristics, thereby expanding their potential applications [11, 12]. Blends make it possible to combine advantageous characteristics of different polymers, generating materials with superior performance and potentially lower costs. Such innovations support circular economy principles and align with sustainable development goals set by the 2030 Agenda.

Among the polymer systems investigated, materials based on polyvinyl alcohol (PVA) and xanthan gum (XG) have attracted attention for applications in packaging, hydrogels, controlled drug release, and dye removal from wastewater [9, 13]. The compatibility between PVA and XG results from hydrogen bonding between their functional groups, enabling the formation of structured and homogeneous films [9, 14]. Nonetheless, studies focusing specifically on PVA/XG blends produced from agro-industrial residues for use in food packaging are still limited.

In this context, the present work aimed to develop and evaluate PVA-based blends containing xanthan gum produced from sugarcane bagasse, a residue generated in large quantities by the Brazilian sugar-energy sector. Beyond providing a renewable source for gum production, the use of this material through fermentation creates opportunities for the valorization of agro-industrial waste and reinforces circular economy strategies associated with SDG 12. Meanwhile, the use of PVA, known for its strong film-forming ability and biodegradability, helps enhance the structural integrity and functional performance of the blends, ensuring better mechanical resistance and barrier properties. The results suggest that this combination can help overcome important limitations of biodegradable materials while contributing to the development of packaging alternatives that are both sustainable and economically attractive. At the same time, the use of xanthan gum derived from sugarcane bagasse provides a valuable destination for agro-industrial residues, reducing waste generation and reinforcing circular economy initiatives associated with the Sustainable Development Goals. Grounded in this context, we hypothesize that blends of PVA with XG derived from sugarcane bagasse can overcome the mechanical and barrier limitations of conventional biodegradable materials, offering a sustainable and cost-effective alternative for food packaging applications.

## 2. Materials and methods

### 2.1. Materials

The materials used for the production of polymer blend films included commercial xanthan gum from Synth (Diadema, Brazil), 200 mesh, and pH (1%) 6–8 with average molecular weight (Mw) of ~2.3 × $10^6$ Da. The laboratory-produced xanthan gum was obtained from sugarcane bagasse extract (6% *w*/*v*) fermented with *Xanthomonas campestris* strain CCT 5268, supplied by the André Tosello Foundation Tropical Culture Collection (Campinas, Brazil), at 28 °C for 120 h, followed by ethanol precipitation and lyophilization. The biopolymer was characterized by average molecular weight, with Mw ~ 1.2 × $10^6$ Da [15]. The films were prepared using polyvinyl alcohol (PVA) from Kuraray Exceval HR-3010 (Tokyo, Japan), with a hydrolysis degree greater than 99% and an average molecular weight ranging from 100,000 to 150,000 g/mol. Glycerol (Sigma-Aldrich, St. Louis, MO, USA, purity ≥ 99.5%, density 1.26 g/mL) was incorporated into the formulations to improve flexibility. Unless otherwise specified, all reagents used in the experimental procedures were analytical grade.

### 2.2. Polymer blend film production and formulations

The polymer blend films were prepared following formulations adapted from [9], which had previously demonstrated homogeneous films with good handling properties. In this study, only two formulations were adopted, as they showed better handling and homogeneous surface. Individual stock solutions of PVA (3% *w*/*w*) and XG (0.5% *w*/*w*) were prepared in 100 mL of deionized water and mixed in defined proportions. For PVA/XGL1, 10 mL of deionized water was added. In all cases, glycerol was added at 30% (*w*/*w*) relative to polymer mass. The blends incorporated either commercial xanthan gum or laboratory-produced xanthan gum obtained from sugarcane bagasse, enabling comparison between the two sources. The formulations are summarized in **Table 1**.

The blends incorporated either commercial xanthan gum or laboratory-produced xanthan gum obtained from sugarcane bagasse, previously characterized for viscosity, molecular weight, Fourier transform infrared spectroscopy (FTIR), Differential scanning calorimetry/thermogravimetric analysis (DSC/TGA), and elemental composition [15].

**Table 1.** Formulation and composition of PVA and polymer blend films.

| Film formulation | PVA volume (mL) | XG volume (mL) | Water volume (mL) | Glycerol (g) |
|---|---|---|---|---|
| PVA | 100 | 0 | 0 | 0.9 |
| PVA/$H_2O$ | 50 | 0 | 50 | 0.45 |
| PVA/XG | 50 | 50 | 0 | 0.525 |
| PVA/XGL1 | 50 | 40 | 10 | 0.51 |
| PVA/XGL2 | 50 | 50 | 0 | 0.525 |

PVA: polyvinyl alcohol; XG: xanthan gum; XGL1, XGL2: sugarcane bagasse-derived xanthan gum variants.

The polymer blend was prepared from separately solubilized PVA and XG solutions. PVA was hydrated in deionized water overnight and then dissolved under stirring (500 rpm) at temperatures between 90 and 95 °C. In a separate step, XG was dispersed in deionized water and kept under continuous agitation at room temperature overnight. Once both solutions became homogeneous, they were mixed and further homogenized, after which glycerol was added to obtain the final film-forming solution. The resulting film-forming solution was cast onto glass plates (20 cm × 30 cm) using a casting method and left to dry naturally by solvent evaporation. Following the drying process, the films were evaluated based on visual and tactile criteria to ensure their suitability for subsequent analyses. These assessments included homogeneity (absence of insoluble particles, bubbles, opacity zones, or color irregularities), continuity (lack of cracks or fractures), handling ability (ease of manipulation without tearing), and flexibility (capacity to bend and fold without rupture). Commercial and laboratory-produced xanthan gums both performed well in PVA-based formulations. In contrast, attempts to produce films using only XG were not successful, as the material did not develop the structural integrity necessary to form cohesive and self-sustaining films. Repeated trials produced gel-like structures that remained poorly dried and adhered strongly to the casting surface, preventing their removal. Two formulations were proposed for laboratory-produced XG (PVA/XGL1 and PVA/XGL2), based on visual and handling properties observed during preliminary tests. **Figure 1** illustrates that the PVA/XG blend films obtained are homogeneous, continuous, and with smooth and uniform surfaces that did not exhibit defects such as pores, cracks, or fissures. **Figure 2** indicates the methodology that was described in the following items.



**Figure 1.** Visual appearance of PVA/XG blend films. PVA: polyvinyl alcohol; XG: xanthan gum.

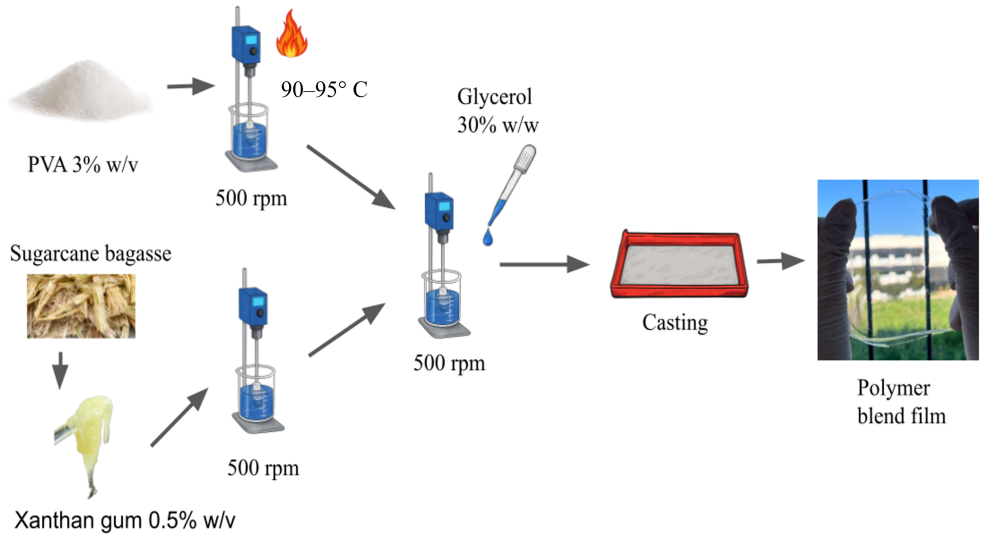



**Figure 2.** Schematic representation of the production of pure polyvinyl alcohol (PVA) and polymer blend films. Adapted from [15]. The arrows indicate the sequence of processing steps, including PVA dissolution, xanthan gum preparation, blending of both solutions with glycerol addition, casting, and film formation.

## 2.3. Characterization of polymeric blend films

Control films and polymeric blend films were stored in a desiccator containing a saturated $Mg(NO_3)_2$ solution at room temperature and 53% relative humidity (RH) for at least 3 days prior to testing [16–18]. **Figure 3** indicates the methodology that will be described in the following items.

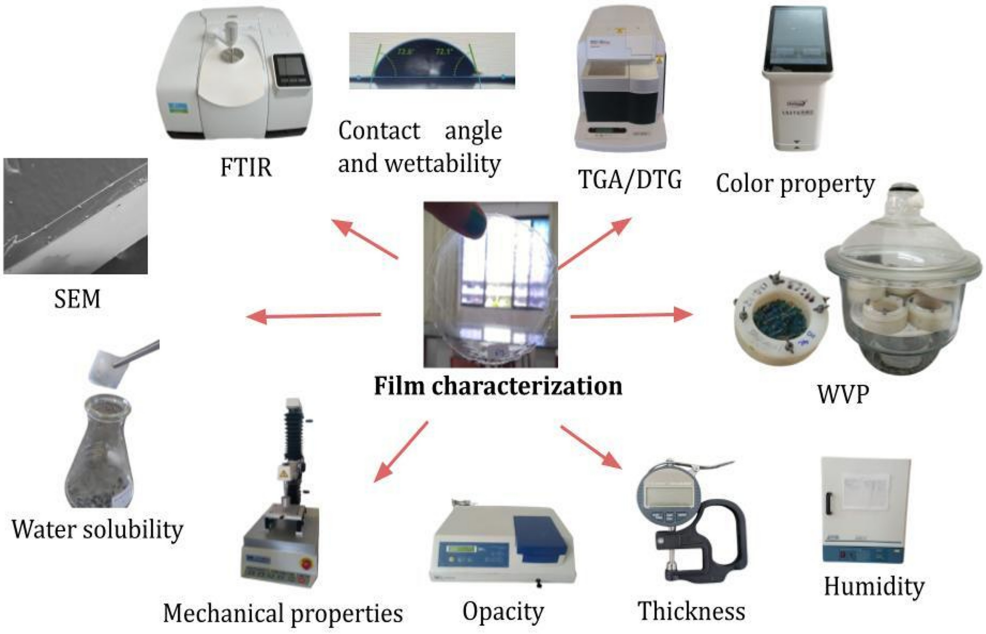



**Figure 3.** Schematic representation of the instruments used for characterization of pure PVA and polymer blend films. PVA: Polyvinyl alcohol; SEM: Scanning electron microscopy; FTIR: Fourier transform infrared spectroscopy; TGA: Thermogravimetric analysis; DTG: Derivative thermogravimetry; WVP: Water vapor permeability. The arrows indicate the characterization analyses performed on the film samples.

### 2.3.1. Thickness

Film thickness was evaluated by taking measurements at five locations distributed across each sample, including the central region and the corners, using a digital micrometer (0.001 mm resolution; 0–12.7 mm range). The average of these measurements was used to represent the thickness of each film [19, 20].

### 2.3.2. Moisture content

Film moisture was evaluated from the mass loss observed after drying. For this purpose, the initial mass of each sample (*mo*) was recorded before the films were kept at 105 °C for 24 h. At the end of the drying period, the samples were weighed again to obtain the final mass ($m_t$) [9]. Moisture content (MC) was then determined according to **Equation (1)**:

$$\text{MC } (\%) = [(mo - mt) / (mo)] \times 100 \quad (1)$$

where *mo* is the mass of the film before drying, and *mt* is the mass after oven drying at 105 °C for 24 h. This procedure was performed in triplicate.

### 2.3.3. Water solubility

Film samples (2 cm × 2 cm) were subjected to a solubility test by initially determining their dry weight (*mo*) after drying at 105 °C for 24 h. The dried specimens were subsequently immersed in 30 mL of deionized water and kept under constant orbital agitation at 50 rpm for 24 h. Following immersion, the residual material was recovered and dried at 105 °C until reaching a stable mass ($m_t$). The samples were then placed in a desiccator to cool before analysis [9, 21]. Dry matter loss was calculated as a percentage of the initial dry mass according to **Equation (2)**:

$$WS \ (\%) = [(mo - mt) / (mo)] \times 100 \quad (2)$$

where *mo* represents the initial dry mass of the sample/film, and *mt* represents the dry mass of the film remaining after filtration, determined after drying to constant weight. This procedure was carried out in triplicate.

### 2.3.4. Color property

The color of the films was measured using a portable Colorimeter LS 173 (Shenzhen Linshang Technology Co., Shenzhen, China), equipped with a D65 light source and operating on the International Commission on Illumination *L*a*b** color space (CIELAB) color scale. The analyses were conducted against a white background, and the parameters analyzed included luminosity (*L*; light–dark), and chromatic coordinates (*a**; red–green) and (*b**; yellow–blue), as well as the overall color difference ($\Delta E$) between samples [20, 22]. Each sample was scanned five times to ensure accuracy and reproducibility. The $\Delta E$ value was calculated to compare the color variation among different formulations, based on the Euclidean distance between two color points in the CIELAB color space (**Equation (3)**):

$$\Delta E = \sqrt{[(L1 - L2)^2 + (a1 - a2)^2 + (b1 - b2)^2]} \quad (3)$$

In this model, *L*, *a**, and *b** are coordinate values derived from a nonlinearly compressed transformation of the XYZ color space defined by the International Commission on Illumination (CIE). A $\Delta E$ value greater than 2 and 3 is considered perceptible to the human eye and is referred to as the Just Noticeable Difference (JND) [23].

### 2.3.5. Transparency/opacity

Film opacity analysis was carried out using a Bel 2000 UV spectrophotometer (Photonics, Milan, Italy) at 600 nm. Rectangular samples measuring 3 cm × 1 cm were obtained, and the thickness of each specimen was determined from five measurements taken at different positions across its surface. The films were placed in cuvette, and absorbance readings were taken. Opacity values were calculated according to **Equation (4)**, which expresses the dependence of opacity on the amount of light passing through the material.

$$\text{Opacity} = A600/x \tag{4}$$

where *A*600 represents the absorbance at 600 nm and *x* corresponds to the average film thickness in mm [22]. Each sample was measured five times for analysis.

### 2.3.6. Thermogravimetric analysis (TGA)

Thermogravimetric curves were used to determine the temperature range that represents the initial and final degradation temperatures of each thermic event. The first derivative of the thermogravimetric (TG, from the English term Thermogravimetric analysis, TGA) curve, known as Derivative thermogravimetry (DTG), was used to determine the rate of mass loss, Tmax (maximum thermal decomposition temperature) of each thermal event, and to identify specific degradation steps and evaluate the thermal stability of the samples. Approximately 2 mg of films was taken on an alumina pan and heated from 50 °C to 600 °C with a heating rate of 10 °C/min under continuous nitrogen gas flow of 50 $cm^3$/min in a DTG—60 H (Shimadzu, Nakagyo-ku, Japan) [24].

### 2.3.7. Fourier transform infrared spectroscopy (FTIR)

To better understand the interactions established within the polymer matrix, the films were analyzed by FTIR spectroscopy [9, 14]. The spectra were recorded from 400 $cm^{-1}$ to 4000 $cm^{-1}$ with a spectral resolution of 4 $cm^{-1}$. A total of 64 scans were collected for each sample, whereas 128 scans were used for background correction. All measurements were performed using a Spectrum 3 FTIR spectrometer (PerkinElmer, Shelton, CT, USA) equipped with a diamond Attenuated Total Reflectance (ATR) accessory [9]. For each film, four spectra were collected from the upper side, and mean values were used for analysis. The analysis focused on two specific absorbance peaks considered representative of the samples [25], the 3273 $cm^{-1}$ band (O-H stretching) and the 1710 $cm^{-1}$ band (C=O stretching), which are associated with hydrogen bonding interactions between PVA and XG [9]. Quantitative evaluation of the selected FTIR signals was carried out by integrating the spectral profiles, with individual linear baselines established for each absorption band. Ratios between peak areas were obtained by dividing the area of one peak by that of another. To evaluate statistical differences among the ratios, Tukey's multiple-range test was applied using a significance criterion of $p < 0.05$. These ratios were used to analyze potential chemical interactions, such as hydrogen bonds, compatibility between PVA and XG, and compare the chemical properties of commercial and lab-produced XG.

### 2.3.8. Mechanical properties

Mechanical performance was assessed through tensile strength (TS) and elongation at break (EB) measurements. The tensile properties of the sample were determined in accordance with ASTM D882 (2018) [26]. The mechanical behavior of the films was assessed with an Instron 5966-E2 universal testing machine (Instron, Norwood, MA, USA), employing specimens prepared with a width of 25.4 mm, equipped with a 1 kN load cell. As specified in ASTM D882 (2018) [26], a 50 mm gauge length and a crosshead speed of 500 mm/min were used for specimens exhibiting an elongation at break greater than 100%, whereas a 100 mm gauge length and a crosshead speed of 50 mm/min were used for specimens exhibiting an elongation at break between 20% and 100%. Five replicates were taken for each film. The distribution pattern of the tensile strength measurements was examined using the Shapiro–Wilk test, which demonstrated that the assumption of normality was not satisfied. However, the variances among the groups were similar, allowing for the application of the non-parametric Mood's median test. This test compares the medians of independent samples and is appropriate when data do not meet the assumptions required for parametric tests such as ANOVA [27].

### 2.3.9. Water vapor permeability (WVP)

The water vapor barrier properties of the films were investigated by measuring Water vapor permeability (WVP) and Water vapor transmission rate (WVTR) using a weight loss-based method adapted from the procedure described in [28] (Standard Test Methods for Water Vapor Transmission of Materials), with specific modifications [28]. For the evaluation, the films were prepared as circular disks with a diameter of 80 mm and subsequently subjected to testing. The specimens were fixed in circular capsules with an effective permeation area of 5.2 cm diameter, which corresponds to the area exposed to both the external environment and the silica gel, thus serving as the permeation interface for the water vapor permeability test. The interior of capsules contains silica gel with low humidity (approximately 0). The capsules were placed in a hermetically sealed desiccator at 25 °C $\pm$ 1 °C, containing a Mg $(NO_3)_2$ solution to maintain 53% relative humidity. Changes in capsule mass were monitored at 24 h intervals for seven days using an analytical balance [29]. All determinations were performed in triplicate. The WVTR was subsequently calculated from the mass gain recorded during the experiment, considering both the exposed film area and the test duration, as defined in **Equation (5)**.

$$\text{WVTR} = m/(A \times t) \tag{5}$$

where WVTR is the Water vapor transmission rate g/m$^2$·day, $m$ (g) is the mass gain of the capsule due to water vapor absorption by the silica gel inside, $A$ is the exposed area of the film (m$^2$), and $t$ is the exposure time (days). Measurements were performed at 24 h intervals. WVTR was expressed in g/m$^2$·day according to the standard convention used for transmission measurements. Water vapor permeability (WVP) was subsequently calculated using **Equation (6)**. Although WVTR is reported on a day basis, WVP is traditionally expressed using hour-based units because the permeability equation incorporates the permeation time in hours. Therefore, the use of both units reflects standard practice in literature and does not affect the comparison of results, since 24 h corresponds to 1 day.

$$\text{WVP} = (\text{WVTR} \times L)/\Delta P \tag{6}$$

For **Equation (5)**, the term WVTR refers to the water vapor transmission rate expressed in g/m$^2$·day. The film thickness is represented by $L$ (m), whereas $\Delta P$ corresponds to the vapor pressure gradient through the film and is given by $S\cdot(R1-R2)$. In this expression, $S$ is the saturation vapor pressure at the experimental temperature

(3.17 kPa), *R*1 is the relative humidity in the external environment (53%), and *R*2 is the relative humidity within the capsule (0%) [29].

### 2.3.10. Water contact angle and wettability analysis

Water contact angle and wettability were used to determine the hydrophilic or hydrophobicity surface properties of the film using the sessile drop method. Distilled water droplets (5 μL) were deposited at room temperature on the surface of the films, and measurements were performed using a Drop Shape Analyzer DSA25 goniometer (Krüss, Hamburg, Germany), using Drop Shape Analysis software (DS4, Krüss GmbH). The contact angle measurements occurred 1 s after the drop was placed in the film surface, while wettability was measured using the average values of the angles obtained between 4 and 55 s. Measurements were performed on different positions and both sides of each film [30]. For statistical reliability, all analyses were conducted in triplicate.

### 2.3.11. Field emission gun scanning electron microscopy (FEG-SEM)

Field emission gun scanning electron microscopy (FEG-SEM) micrographs were obtained to analyze the morphology of the films in two distinct regions: the surface and the cross-sectional area. These images were used to identify structural features such as flaws, phase separation, polymer agglomeration, or other morphological irregularities. For cross-sectional analysis, the specimens were first immersed in liquid nitrogen and fractured. Both the surface and cross-sections were coated with a thin layer of gold via vapor deposition to enhance conductivity. The samples were examined using a CLARA Scanning Electron Microscope (TESCAN, Brno, Czech Republic) under high vacuum conditions, operated at 20 kV with 500× magnification [9, 29].

## 2.4. Statistical analyses

Replicated measurements were performed for all analyses, and the data are reported as mean ± standard deviation. The statistical significance of differences among treatments was verified by ANOVA, with Tukey's test subsequently applied for multiple comparisons at the 5% significance level ($p < 0.05$).

# 3. Results

## 3.1. Production of polymer blend films

Polymer blend films were cast, based on the methodology of [9]. The chosen formulation was in accordance with the characteristics of continuity (maintaining structural integrity throughout drying, with no observable cracks or breaks) and homogeneity (exhibiting a uniform appearance, without visible solid residues, particulate matter, or heterogeneous regions characterized by color or opacity variations), in addition to maneuverability (possibility of being handled without risk of rupture), as recommended by [31, 32]. **Figure 4** illustrates the PVA and polymer blend films.

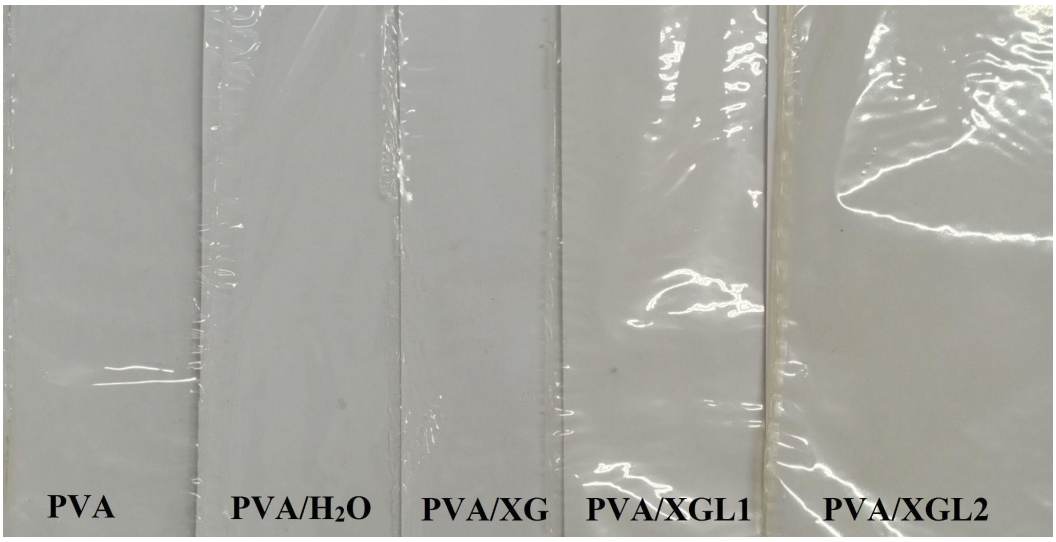



**Figure 4.** Images of polymer blend films composed of polyvinyl alcohol (PVA) and xanthan gum (XG), produced via solvent casting. XGL1, XGL2: sugarcane bagasse-derived xanthan gum variants.

## 3.2. Characterization of films and polymer blend films

### 3.2.1. Thickness, moisture content, and solubility

The values obtained for thickness, moisture content, and water solubility are presented in **Table 2**. All films exhibited typical characteristics of PVA-based materials, such as flexibility, homogeneity, and transparency, although the blends containing xanthan gum appeared more opaque. The thickness of the polymer blend films ranged from 0.059 mm to 0.064 mm, with no significant differences among them ($p < 0.05$). However, the pure PVA film showed a significantly higher thickness (0.125 mm), which can be attributed to its higher polymer concentration and proportionally greater plasticizer content. In contrast, the PVA/$H_2O$ formulation, which contained less PVA and additional water, resulted in a thinner film, similar to the blends. This confirms that polymer concentration and water content directly influence film thickness.

**Table 2.** Thickness, moisture content, and solubility of PVA and polymer blend films.

| Film | Thickness (mm) | Moisture content (%) | Solubility (%) |
|---|---|---|---|
| PVA | 0.125 ± 0.012 $^{b}$ | 27.95 ± 1.19 $^{a}$ | 7.82 ± 0.59 $^{b}$ |
| PVA/$H_2O$ | 0.061 ± 0.001 $^{a}$ | 11.70 ± 0.82 $^{c}$ | 6.88 ± 0.56 $^{a}$ |
| PVA/XG | 0.063 ± 0.003 $^{a}$ | 11.48 ± 0.56 $^{d}$ | 9.76 ± 0.45 $^{c}$ |
| PVA/XGL1 | 0.064 ± 0.002 $^{a}$ | 12.65 ± 0.13 $^{b}$ | 10.33 ± 0.39 $^{d}$ |
| PVA/XGL2 | 0.059 ± 0.003 $^{a}$ | 11.31 ± 0.31 $^{e}$ | 11.34 ± 0.63 $^{e}$ |

Within each column, means sharing the same letter belong to the same statistical group and are not significantly different according to Tukey's multiple comparison test. Means with different letters belong to different statistical groups and differ significantly at the 5% significance level ($p < 0.05$). PVA: polyvinyl alcohol; XG: xanthan gum; XGL1, XGL2: sugarcane bagasse-derived xanthan gum variants.

In this study, moisture content varied significantly among all samples ($p < 0.05$). The pure PVA film exhibited the highest moisture content (27.95%), likely due to its greater thickness and the hydrophilic nature of PVA, which favors water retention. In the PVA/$H_2O$ formulation, moisture content dropped sharply to 11.70%. This reduction can be attributed to hydrogen bonding established between water molecules and the hydroxyl groups of PVA during film formation, which restricted the amount of free water and promoted a denser, less hygroscopic structure. Additionally, the lower polymer concentration and thinner film structure reduced the capacity for water entrapment.

The results obtained here agree with those reported by [9], who observed that the addition of xanthan gum to PVA films led to lower moisture content. This behavior is commonly associated with hydrogen bond interactions between the polymers, which reduce the availability of hydroxyl groups for interaction with water. Consequently, moisture retention decreases as xanthan gum is incorporated into the matrix. In contrast, pure PVA films evaluated by [9] exhibited higher moisture content (11.95%), reinforcing the trend found in the present work.

The addition of commercial xanthan gum (PVA/XG) resulted in intermediate moisture content (11.48%), slightly higher than PVA/$H_2O$, possibly due to its higher polymer and plasticizer content, which may have increased free volume and water permeability. Among the laboratory-produced gums, PVA/XGL1 exhibited higher moisture content (12.65%) than PVA/XGL2 (11.31%). These differences are likely due to the variation in the amount of xanthan gum and water used in each formulation, since both gums were produced under identical conditions. The higher water content and lower plasticizer concentration in PVA/XGL1 may have promoted stronger hydrogen bonding and a denser polymer network.

Water solubility is another critical property, as it reflects the water resistance of polymer films and plays an important role in determining their biodegradability and suitability for packaging applications [20, 33]. Solubility varied significantly among the formulations ($p < 0.05$). The pure PVA film showed the lowest solubility (7.82%), likely due to its dense hydrogen bonding network and reduced water diffusion. The PVA/$H_2O$ film exhibited even lower solubility (6.88%), suggesting that the interactions between water and PVA during film formation led to a more compact and less soluble structure. In contrast, the addition of xanthan gum increased solubility, especially in the laboratory-produced variants. PVA/XGL1 and PVA/XGL2 showed solubility values of 10.33% and 11.34%, respectively, with the latter being the most soluble and also the thinnest film. This behavior may be linked to the higher plasticizer content and lower hydrogen bonding in XGL2, which facilitated water penetration and film dissolution.

These results diverge from those of [9], who reported that pure PVA films had the highest solubility (76.77%) due to their polar structure and abundance of hydroxyl groups. In their study, the incorporation of XG decreased solubility by restricting polymer chain mobility through intermolecular interactions. However, they also noted that excessive XG could increase solubility due to the hydrophilic nature of the biopolymer. In the present study, the opposite fact was observed, the addition of XG (commercial or lab-produced) led to an increase in solubility compared to pure PVA. Differences in the proportion of polymers used, drying approach, and the inherent hydrophilic behavior of xanthan gum help explain this variation.

Overall, the results suggest that the structural and functional characteristics of the films are strongly influenced by the formulation adopted, especially the polymer composition, the amount of water used during processing, the source and concentration of xanthan gum, and the plasticizer content. The presence of water during blend preparation, as in PVA/$H_2O$ and PVA/XGL1, appears to promote hydrogen bonding and compactness, reducing moisture and solubility. In contrast, formulations without added water and with higher plasticizer content, such as PVA/XGL2, tend to be more permeable and soluble.

The laboratory-produced xanthan gum exhibited a molecular weight of $1.2 \times 10^6$ Da, slightly lower than the commercial sample (~$2.3 \times 10^6$ Da), but both showed similar rheological behavior and pseudoplasticity. Thermal analysis revealed comparable stability, with decomposition temperatures of 290 °C (lab-produced) and 300 °C (commercial). FTIR spectra suggested structural similarity, with minor differences attributed to the fermentation substrate. These results indicate that xanthan gum obtained from sugarcane bagasse can be considered a viable alternative to commercial XG for incorporation into PVA-based films, with the added advantage of being produced from agro-industrial waste at lower cost.

### 3.2.2. Color property

**Table 3** presents the color property ($L$, $a^*$, and $b^*$) of the films and polymer blend formulations, along with the total color difference ($\Delta E$) among them. Color and transparency are essential attributes in food packaging, as they directly influence consumer perception, especially regarding the freshness and quality of the product [4, 34, 35]. The color characteristics of the films were assessed using the CIELAB color system. In this color space, $L$ represents luminosity, where increasing values indicate a lighter appearance. The chromatic coordinate $a^*$ varies from green ($-a^*$) to red ($+a^*$), while b* ranges from blue ($-b^*$) to yellow ($+b^*$) [20]. Pure PVA film was used as the control, showing the lightest ($L$ = 92.13) due to its transparent nature.

**Table 3.** Color properties ($L^*$, $a^*$, and $b^*$) and total color difference ($\Delta E$) of PVA and polymer blend films.

| Film | $L^*$ | $a^*$ | $b^*$ | $\Delta$E |
|---|---|---|---|---|
| PVA | 91.13 ± 0.08 $^{e}$ | 1.63 ± 0.14 $^{a}$ | −1.21 ± 0.44 $^{a}$ | - |
| PVA/$H_2O$ | 92.17 ± 0.08 $^{d}$ | 1.63 ± 0.18 $^{a}$ | −1.16 ± 0.35 $^{b}$ | 0.50 ± 0.12 $^{a}$ |
| PVA/XG | 91.44 ± 0.08 $^{c}$ | 1.68 ± 0.10 $^{b}$ | −0.65 ± 0.51 $^{c}$ | 0.96 ± 0.50 $^{b}$ |
| PVA/XGL1 | 90.67 ± 0.08 $^{b}$ | 2.03 ± 0.09 $^{c}$ | −2.53 ± 0.26 $^{d}$ | 4.04 ± 0.43 $^{c}$ |
| PVA/XGL2 | 89.95 ± 0.08 $^{a}$ | 2.53 ± 0.6 $^{d}$ | −3.93 ± 0.37 $^{e}$ | 5.66 ± 0.77 $^{d}$ |

Within each column, means sharing the same letter belong to the same statistical group and are not significantly different according to Tukey's multiple comparison test. Means with different letters belong to different statistical groups and differ significantly at the 5% significance level ($p < 0.05$). PVA: polyvinyl alcohol; XG: xanthan gum; XGL1, XGL2: sugarcane bagasse-derived xanthan gum variants.

The PVA/$H_2O$ formulation exhibited minimal color variation ($\Delta E$ = 0.50), maintaining a similar appearance to the control. When commercial xanthan gum was added, the resulting film remained light ($L$ = 91.44) and showed a slight color change ($\Delta E$ = 0.96), with reduced blueness. However, films produced with laboratory-produced xanthan gum exhibited increased redness and yellowness due to the natural color of the biopolymer, and consequently the sugarcane bagasse. These formulations showed lower lightness values ($L^*$ = 90.67 for PVA/XGL1 and $L^*$ = 89.95 for PVA/XGL2), although they still maintained a visually light appearance. Particularly, the formulation with higher XG content (PVA/XGL2) showed greater redness ($a^*$ = 2.53) and yellowness ($b^*$ = 3.93), with significant color differences compared to pure PVA films ($\Delta E$PVA/XGL1 = 4.04 and $\Delta E$PVA/XGL2 = 5.66).

These optical differences may be explained by the structural organization of the polymer blends. In the PVA/XGL1 formulation, the presence of water appears to have contributed to a more amorphous polymer structure, which enhanced the transparency of the film. The combination of water and plasticizer may have interfered in the molecular packing, leading to the formation of additional voids between polymer chains and reducing structural

order. These irregular arrangements could allow light to pass through more easily, resulting in a clearer film. In contrast, the PVA/XGL2 film may have formed more organized molecular interactions, due to the higher XG content, leading to reduced transparency. This behavior suggests a more crystalline structure, with tightly packed chains and fewer voids. The increased tendency toward red and yellow tones in this formulation may also contribute to its opaque appearance.

### 3.2.3. Optical properties (transmittance and opacity)

The analysis of optical properties (transmittance and opacity) evaluates the impact of components on the films. In general, higher opacity values correspond to lower transmittance, indicating reduced transparency [36]. **Table 4** presents the opacity and transmittance values of pure PVA and polymer blend films. Changes in film transparency were also observed after the incorporation of xanthan gum and the other formulation components. These changes are likely related to modifications in the internal structure of the polymeric network, which directly affect how light passes through the material [4], as illustrated in **Figure 5**.

**Table 4.** Optical properties (opacity and transmittance at 600 nm) of PVA and polymer blend films.

| Film | Opacity at 600 nm (*A*600/mm) | Transmittance (%) 600 nm |
|---|---|---|
| PVA | 16.40 ± 1.84 $^{a}$ | 91.55 ± 0.33 $^{e}$ |
| PVA/$H_2O$ | 32.14 ± 0.76 $^{d}$ | 91.20 ± 0.22 $^{d}$ |
| PVA/XG | 31.26 ± 1.37 $^{c}$ | 87.73 ± 0.40 $^{c}$ |
| PVA/XGL1 | 29.90 ± 0.66 $^{b}$ | 86.18 ± 0.553 $^{b}$ |
| PVA/XGL2 | 32.80 ± 1.68 $^{e}$ | 85.43 ± 0.13 $^{a}$ |

Within each column, means sharing the same letter belong to the same statistical group and are not significantly different according to Tukey's multiple comparison test. Means with different letters belong to different statistical groups and differ significantly at the 5% significance level ($p < 0.05$). PVA: polyvinyl alcohol; XG: xanthan gum; XGL1, XGL2: sugarcane bagasse-derived xanthan gum variants; *A*600: absorbance of the film measured at 600 nm.

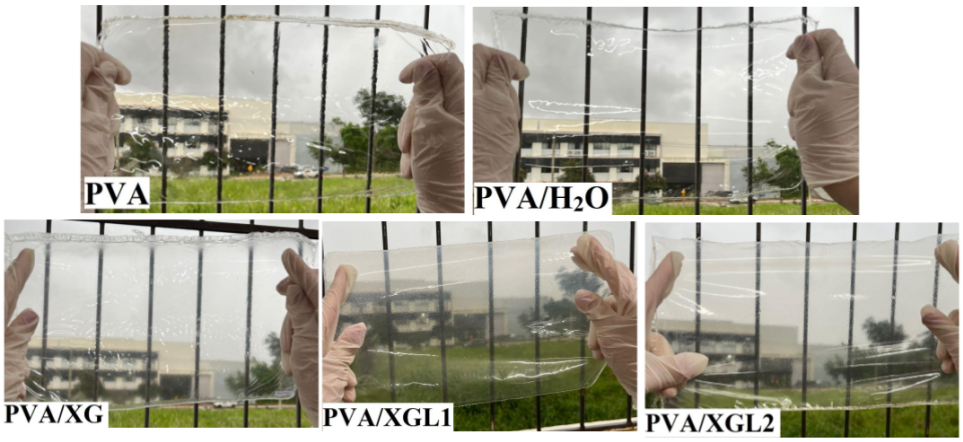



**Figure 5.** Images of transparency and surface uniformity of PVA and polymer blend films. From left to right: PVA, PVA/$H_2O$, PVA/XG, PVA/XGL1, and PVA/XGL2. All films were produced by solvent casting and have approximate dimensions of 20 cm × 30 cm. PVA: polyvinyl alcohol; XG: xanthan gum; XGL1, XGL2: sugarcane bagasse-derived xanthan gum variants.

All polymer blend films exhibited transmittance values above 80% at 600 nm, indicating that they are transparent according to standard classification. Pure PVA films exhibited the highest transmittance (91.55%), confirming their highly transparent nature and superior light transmission compared to the polymer blends. After the addition of XG, both commercial and laboratory-produced, transmittance decreased (87.73%, 86.18%, and 85.43%, respectively), while opacity increased. This reduction in transparency is likely due to the incorporation of XG into the matrix, which alters the spatial arrangement of polymer chains and increases light scattering, resulting in a denser and less light-permeable structure.

From a consumer perspective, higher opacity may negatively influence visual appeal and product selection, especially in food packaging where clarity is associated with freshness. Chen et al. [9] reported similar findings, with pure PVA films showing significantly higher transmittance (91.90%) than composite films (89.40% and 85.40% for PVA/XGL1 and PVA/XGL2, respectively). The values reported by [9] are consistent with those found in this study.

The reduced transmittance in the blends may be attributed to the presence of XG that promotes more organized or compact molecular arrangements, depending on its concentration and hydration state, which affects how light passes through the material. This interpretation aligns with the color analysis, where increased red and yellow tones were associated with greater opacity.

According to [4], materials with transmittance above 80% at 600 nm are considered transparent, while those above 90% are classified as highly transparent. Among the polymeric materials frequently used for food packaging purposes are polycarbonate (PC), polymethyl methacrylate (PMMA), polystyrene (PS), polyvinyl chloride (PVC), and polyvinyl alcohol (PVA), all of which can provide suitable optical characteristics. Based on their light transmission behavior, materials are generally classified as translucent when transmittance ranges from 10% to 80%, while values lower than 10% indicate an opaque material.

Importantly, while visible light transmission is essential for consumer evaluation of product freshness, blocking ultraviolet (UV) radiation is desirable, as UV exposure is one of the main causes of food degradation [22]. In this context, the use of biopolymers derived from agro-industrial residues, such as those used in this study, offers a dual benefit: they allow sufficient transmission of visible light for product visibility while potentially reducing UV transmittance, contributing to product protection and shelf-life extension.

### 3.2.4. Thermogravimetric analysis (TGA)

The thermal behavior of pure PVA and the blended films was evaluated by TG and DTG analyses (**Figure 6a,b**), and the thermal events are summarized in **Table 5**. All formulations exhibited the typical multistep degradation profile reported for PVA- and polysaccharide-based materials, involving moisture loss, degradation of the polymer matrix, and decomposition of intermediate carbonaceous structures. Similar behavior has been described for PVA/xanthan gum films, starch/PVA blends, and other biodegradable packaging materials [9, 37, 38].

The first degradation stage, observed below approximately 210 °C, was associated with the release of free and bound water from the polymer network. The variation in mass loss among formulations indicates differences in water retention, which are directly influenced by hydrogen bond interactions within the matrix. In this sense, the lower mass losses observed for PVA/XGL1 and PVA/$H_2O$ suggest reduced moisture retention and a more organized structure, which may contribute to better dimensional stability during storage. Similar effects have been reported for starch/PVA and xanthan gum-based films [39].

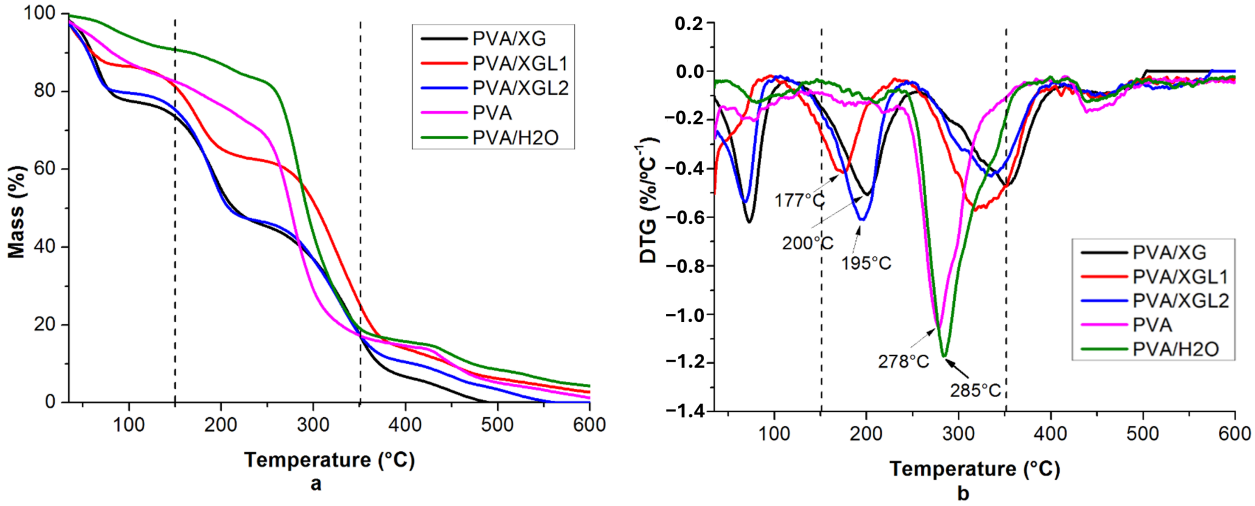



**Figure 6.** TG (**a**) and DTG (**b**) thermograms of the PVA- and polymer-based films. TG: Thermogravimetric curve; DTG: Derivative thermogravimetry; PVA: polyvinyl alcohol; XG: xanthan gum; XGL1, XGL2: sugarcane bagasse-derived xanthan gum variants. The vertical dashed lines indicate the temperature regions used as references for comparing the degradation events among the different film formulations.

The second thermal event corresponded to the main degradation of the polymer structure. Pure PVA and PVA/$H_2O$ showed higher Tmax values than the xanthan gum-containing films, indicating greater thermal resistance. The earlier degradation observed in the blends is attributed to the lower thermal stability of xanthan gum, whose glycosidic bonds and side-chain groups are more susceptible to thermal cleavage than the PVA backbone. This behavior is consistent with previous reports on PVA/xanthan gum composites and active biodegradable films, where the incorporation of natural polysaccharides alters degradation pathways through intermolecular interactions and hydrogen bonding [9, 13].

The third degradation stage occurred at higher temperatures and was related to the decomposition of intermediate carbonaceous products formed during the previous degradation step. This event accounted for a significant fraction of the overall mass loss, particularly for PVA/XG and PVA/XGL1, indicating progressive breakdown of the remaining polymer structure. A similar degradation mechanism has been reported for starch/PVA blends and electrospun PVA-based materials [37, 38].

An important aspect of these results is the distinction between stage-specific and cumulative mass loss. The percentages reported in **Table 5** represent the mass lost during each individual degradation event and should not be interpreted as residual mass values. When all thermal events are considered together, the residual mass at 600 °C ranged from 0 to 4.5%. The absence of residue in PVA/XG and PVA/XGL2 indicates almost complete thermal decomposition, while PVA, PVA/$H_2O$, and PVA/XGL1 produced only small amounts of thermally stable residue. Similar low-residue behavior has been reported for biodegradable films based on PVA and natural polysaccharides [37, 39].

From a practical standpoint, the observed thermal behavior supports the potential use of these materials in food packaging applications. Although xanthan gum reduced the temperature associated with the onset of degradation, all formulations remained stable at temperatures far above those encountered during processing, storage, and use. Furthermore, the low residual mass after heating reinforces the predominantly organic and biodegradable nature of the films and suggests a reduced tendency for persistent residue formation after disposal. Thus, the TG/DTG curves and the values presented in **Table 5** are fully consistent, since the reported

percentages correspond to individual degradation events, whereas the residual masses represent only the material remaining after the cumulative degradation process up to 600 °C.

**Table 5.** Thermal events, temperature range, Tmax and weight loss of the PVA and polymer blend films.

| Film | Thermal event | Temperature range (°C) | Tmax (°C) | Weight loss (%) |
|---|---|---|---|---|
| PVA | Polymer dehydration | 35–211 | 78 | 22 |
| | Polymer degradation | 218–393 | 278 | 58 |
| | Pyrolysis | 402–535 | 438 | 12 |
| | Residue (600 °C) | | | 1.3 |
| PVA/$H_2O$ | Polymer dehydration | 35–211 | 77 | 12 |
| | Polymer degradation | 222–386 | 285 | 68 |
| | Pyrolysis | 405–520 | 440 | 8 |
| | Residue (600 °C) | | | 4.5 |
| PVA/XG | Polymer dehydration | 35–121 | 73 | 20.5 |
| | Polymer degradation | 121–262 | 200 | 33 |
| | Pyrolysis | 267–421 | 352 | 38 |
| | Residue (600 °C) | | | 0 |
| PVA/XGL1 | Polymer dehydration | 35–119 | 85 | 12 |
| | Polymer degradation | 122.5–245 | 117 | 23 |
| | Pyrolysis | 253–441.5 | 315 | 51 |
| | Residue (600 °C) | | | 1.3 |
| PVA/XGL2 | Polymer dehydration | 35–128 | 67 | 19 |
| | Polymer degradation | 133–263 | 195 | 34 |
| | Pyrolysis | 265.5–443 | 330 | 36 |
| | Residue (600 °C) | | | 0 |

PVA: polyvinyl alcohol; XG: xanthan gum; XGL1, XGL2: sugarcane bagasse-derived xanthan gum variants; Tmax: temperature at which the maximum rate of mass loss occurs during a thermal degradation event.

### 3.2.5. FTIR

The FTIR spectra of pure PVA and the blended films are presented in **Figure 7**. Pure PVA exhibited the characteristic absorption bands expected for this polymer, confirming that its chemical structure was preserved after film formation. No additional absorption bands appeared after xanthan gum incorporation, indicating that blending did not involve the formation of new covalent bonds. Instead, the spectral changes observed suggest that xanthan gum modified the molecular arrangement of the PVA chains through intermolecular interactions. Similar behavior has been reported for PVA-based systems containing polysaccharides, in which compatibility between the components is primarily governed by secondary interactions that promote network formation and matrix cohesion [9, 38].

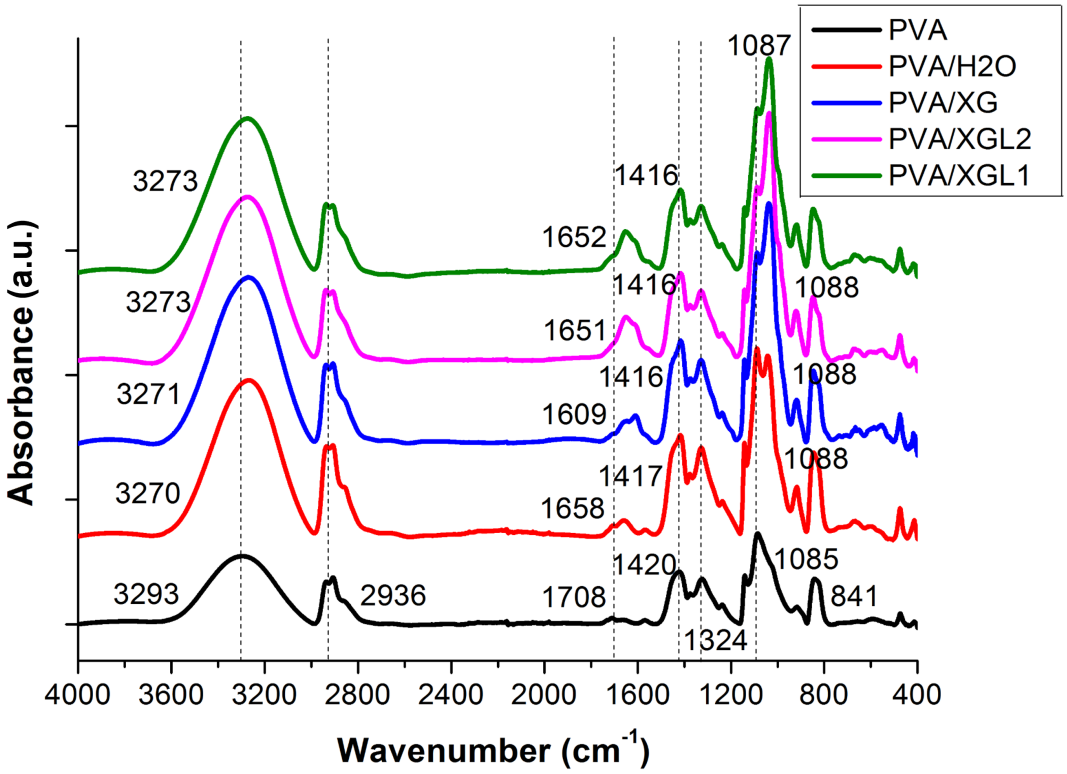



**Figure 7.** Pure PVA and polymer blend film spectra. PVA: polyvinyl alcohol; XG: xanthan gum; XGL1, XGL2: sugarcane bagasse-derived xanthan gum variants. The vertical dashed lines identify the main absorption bands used to evaluate spectral changes and peak shifts resulting from interactions between PVA and xanthan gum in the film matrices.

The most pronounced changes occurred in the hydroxyl region. While pure PVA presented the O-H stretching band at 3293 $cm^{-1}$, the blended films exhibited this absorption between 3270 and 3273 $cm^{-1}$. This displacement toward lower wavenumbers indicates a strengthening of intermolecular associations, since hydroxyl groups involved in hydrogen bonding vibrate at lower energies. The observed shift therefore suggests that hydroxyl groups from PVA interacted with hydroxyl, carboxylate, and carbonyl groups present in xanthan gum. Similar reductions in O-H stretching frequency have been reported for PVA/xanthan gum films, PVA/starch systems, and other polysaccharide-based biodegradable materials, where enhanced molecular interactions improved blend compatibility and structural cohesion [9, 13, 38].

Additional evidence of these interactions was found in the carbonyl region. The C=O absorption band shifted from 1708 $cm^{-1}$ in pure PVA to values between 1609 and 1658 $cm^{-1}$ in the blended films. Such displacement indicates that carbonyl-containing groups also became involved in the intermolecular association process. As these groups participate in stronger interactions with neighboring chains, the vibrational energy of the carbonyl bond decreases, resulting in the shift toward lower wavenumbers. Comparable behavior has been described for several PVA/polysaccharide blends, where carbonyl groups act as hydrogen bond acceptors and contribute to the stabilization and organization of the polymer network [37].

The analysis of the OH/C=O ratio (**Figure 8**) supports this interpretation. The progressive increase in this parameter from pure PVA to the xanthan gum-containing formulations indicates a greater participation of hydroxyl-rich domains in the intermolecular interaction network. The highest values observed for PVA/XGL1 and PVA/XGL2 suggest a higher density of interaction sites, which is consistent with the spectral shifts observed in both the hydroxyl and carbonyl regions.

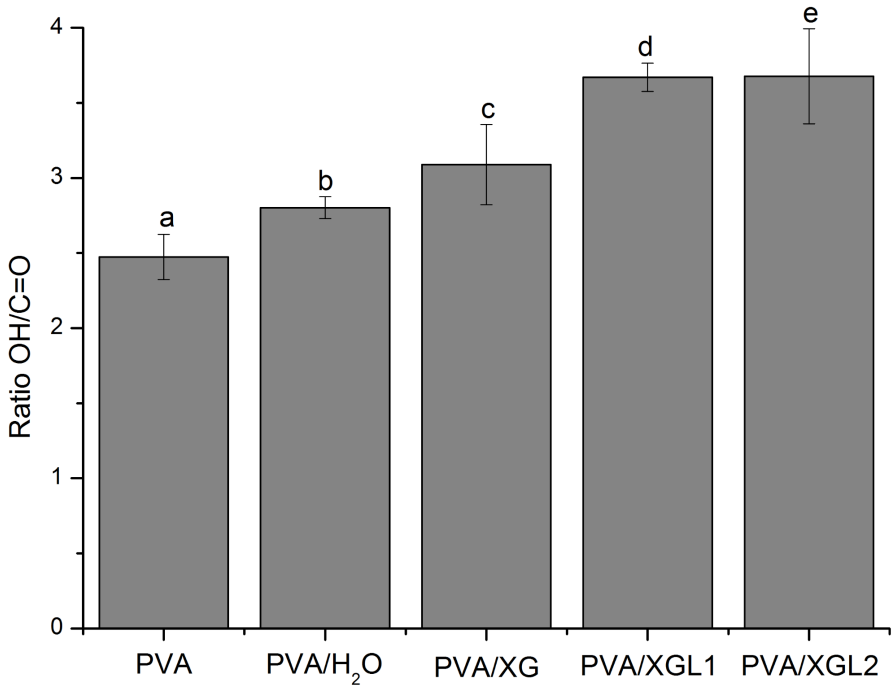



**Figure 8.** FTIR analysis of the OH/C=O ratio of pure PVA and polymer blend films. Error bars represent the standard deviation of the measurements. Different letters indicate different statistical groups according to Tukey's multiple comparison test. Samples sharing the same letter are not significantly different, whereas samples with different letters differ significantly at the 5% significance level ($p < 0.05$). PVA: polyvinyl alcohol; XG: xanthan gum; XGL1, XGL2: sugarcane bagasse-derived xanthan gum variants.

Taken together, the FTIR results indicate that xanthan gum promotes molecular rearrangement within the PVA matrix by increasing the extent of intermolecular association. As a consequence, the polymer chains become more integrated, generating a more cohesive and interconnected structure (**Figure 9**). Similar relationships between FTIR band shifts, hydrogen bond formation, and enhanced film performance have been reported for PVA/starch films, PVA/xanthan gum composites, and other biodegradable packaging materials [9, 13, 37, 38]. Therefore, the simultaneous displacement of the O-H and C=O bands toward lower wavenumbers, together with the increase in the OH/C=O ratio, provides strong evidence that intermolecular interactions are responsible for

the good compatibility between PVA and xanthan gum and likely contribute to the structural and functional improvements observed in the blended films.

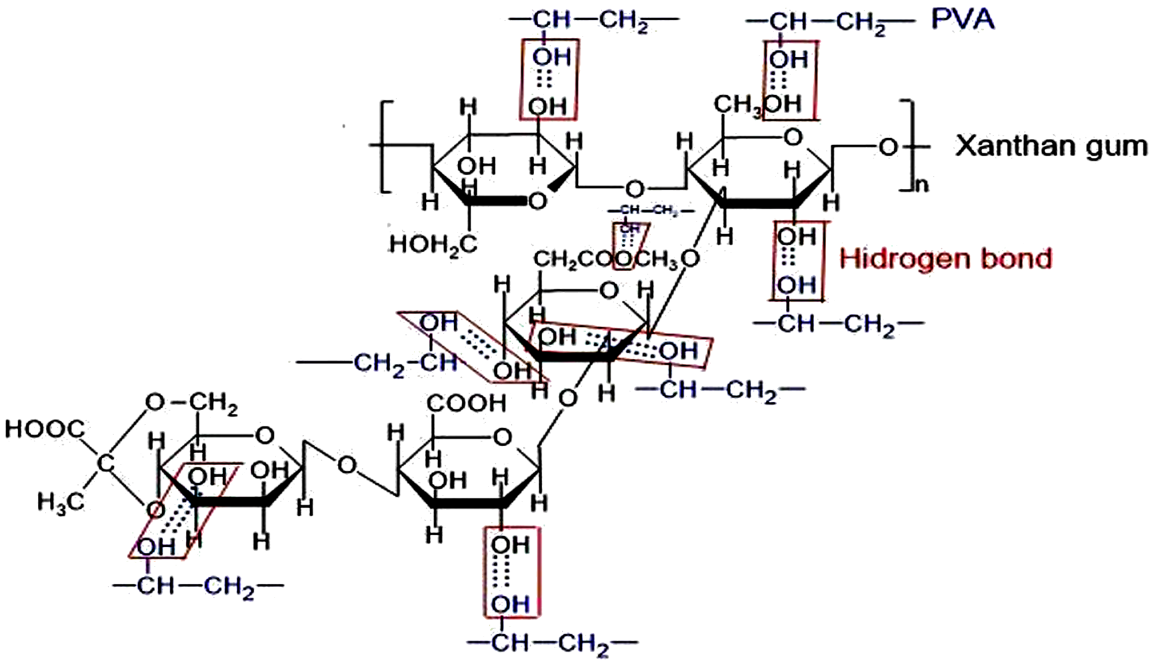



**Figure 9.** Schematic representation of the proposed intermolecular interactions between polyvinyl alcohol (PVA) and xanthan gum (XG). Adapted from [14]. Dashed lines indicate the proposed hydrogen-bonding interactions between hydroxyl and carboxyl-containing functional groups, while the highlighted regions identify the main interaction sites.

### 3.2.6. Mechanical analysis

As shown in **Figure 10**, the tensile strength data did not satisfy the normality assumption according to the Shapiro-Wilk test; therefore, the results were evaluated using the non-parametric Mood's median test [27]. Among the formulations investigated, the PVA/$H_2O$ film exhibited the highest tensile strength (47.03 MPa), whereas the PVA/XGL2 film showed the lowest value (20.70 MPa). The wider error bar observed for the PVA/$H_2O$ film suggests greater variability among replicates, possibly associated with local heterogeneities developed during film formation or differences in water distribution within the polymer matrix.

The mechanical performance of the films appears to be closely related to the role of water during blend preparation. The incorporation of commercial xanthan gum (XG) without additional water resulted in a tensile strength comparable to that of neat PVA, suggesting limited contribution of the polysaccharide to the reinforcement of the matrix. This behavior may be attributed to insufficient hydration of xanthan gum, restricting its dispersion and interaction with PVA chains.

In contrast, the PVA/XGL1 formulation, prepared with laboratory-produced xanthan gum in the presence of water, exhibited higher tensile strength while maintaining satisfactory flexibility. This result suggests that water promoted the hydration and dispersion of xanthan gum, favoring intermolecular interactions and the formation of a more homogeneous and cohesive polymer network. Conversely, the lower tensile strength observed for the PVA/XGL2 film indicates that the absence of water may have hindered polysaccharide incorporation, leading to

a less uniform structure and reduced stress transfer. Overall, these findings highlight the key role of water in the organization of the polymer network and the resulting mechanical performance of the films.

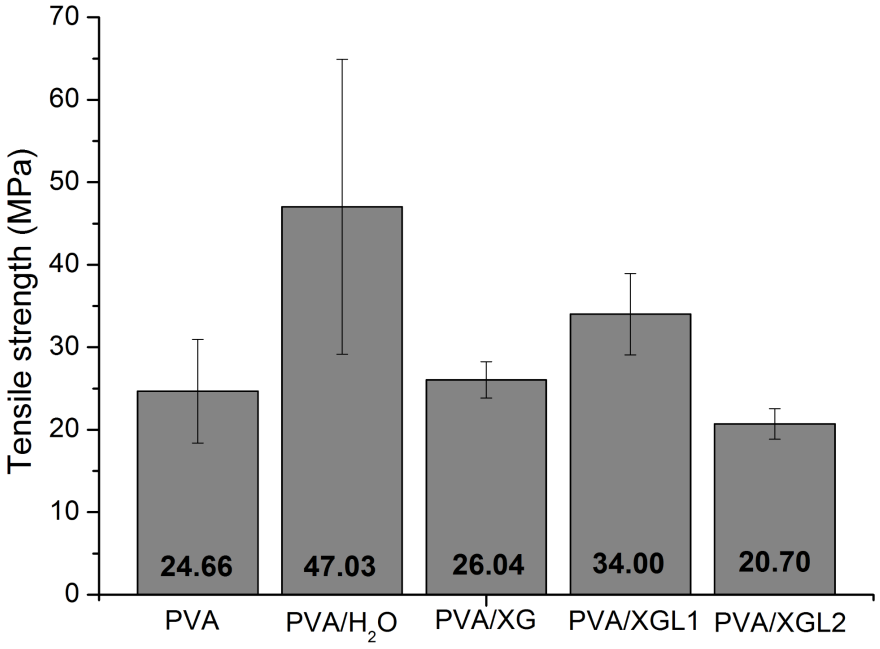



**Figure 10.** Tensile strength of PVA and polymer blend films. Values are expressed as mean ± standard deviation, and the error bars represent the standard deviation of the measurements. PVA: polyvinyl alcohol; XG: xanthan gum; XGL1, XGL2: sugarcane bagasse-derived xanthan gum variants.

The mechanical behavior of the films is closely linked to molecular interactions within the polymer matrix. The addition of water to PVA films containing plasticizers led to an approximately 50% increase in tensile strength, resulting in enhanced hydrogen bonding and network cohesion. However, this increase was accompanied by reduced flexibility, as the denser structure limited chain mobility.

The elongation at break values are shown in **Figure 11**. The pure PVA film exhibited the highest elongation (432.14%), consistent with its flexibility and chain mobility. This behavior is attributed to the interactions between PVA molecular chains via hydrogen bonds, which increase interstitial volume and reduce intermolecular forces, allowing greater deformation under stress [40, 41]. The PVA/$H_2O$ film had lower elongation (285.81%) but maintained good flexibility, due to water-enhanced hydrogen bonding. Among the blends, the PVA/XGL1 film exhibited an elongation at break of 270.97%, outperforming PVA/XG and PVA/XGL2 (109.15% and 131.02%, respectively), without added water and showed reduced chain mobility.

The mechanical performance was affected by the concentrations of xanthan gum, plasticizer, and water used during blend formation. In the PVA/XGL1 formulation, the lower content of XG and plasticizer, combined with the presence of water, contributed to stronger hydrogen bonding and a more cohesive polymer network. This outcome is consistent with observations by [9], who noted that excessive gum content can interfere with the structural integrity of PVA, leading to diminished mechanical strength.

Gomes et al. [42] reported that the incorporation of xanthan gum derived from sugarcane bagasse improved the flexibility of starch-based films and increased their tensile strength by more than 45%. However, a significant reduction, greater than 70%, was observed in elongation at break, indicating that the structural reinforcement came at the expense of flexibility. Similarly, Tavassoli et al. [37] produced pure PVA films using different sonication

times and achieved tensile strength and elongation values of 25.50 MPa and 29.6%, respectively, for films treated with 7.5 min of ultrasonication.

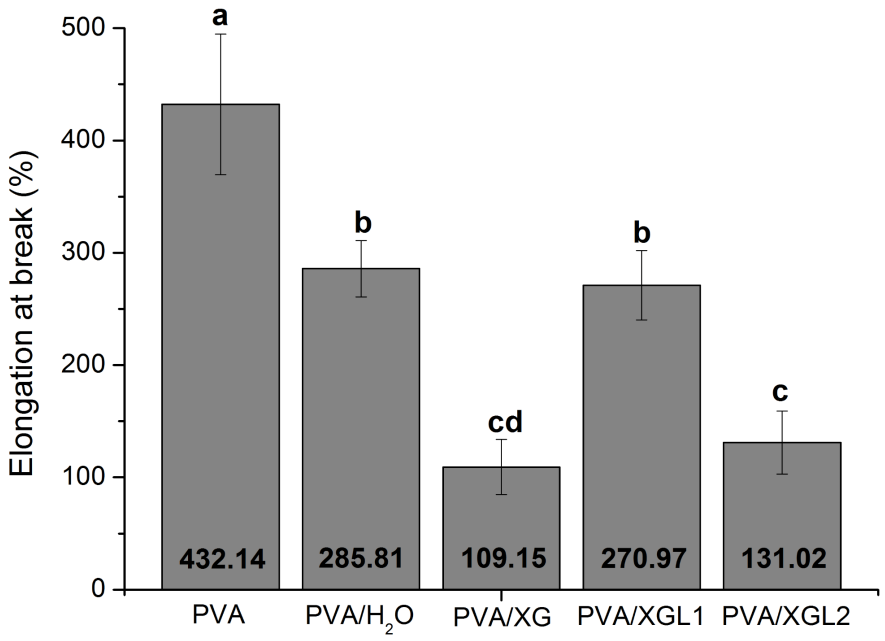



**Figure 11.** Elongation at break of PVA and polymer blend films. Error bars represent the standard deviation of the measurements. Different letters indicate different statistical groups according to Tukey's multiple comparison test. Samples sharing the same letter are not significantly different, whereas samples with different letters differ significantly at the 5% significance level ($p < 0.05$). PVA: polyvinyl alcohol; XG: xanthan gum; XGL1, XGL2: sugarcane bagasse-derived xanthan gum variants.

When compared to commercial polymers such as HDPE and PP, commonly used in flexible packaging, the PVA/XGL1 film demonstrates a more balanced mechanical profile. According to [43], HDPE films typically show tensile strength around 25–30 MPa and elongation above 500%, while PP ranges from 30–40 MPa to 100–600%. Although these materials offer high flexibility, their tensile strength is generally lower than that of PVA/XGL1. By combining elevated strength with substantial elongation, this formulation presents a promising alternative for packaging applications requiring both durability and flexibility. It should be noted, however, that the incorporation of xanthan gum into PVA matrices affected mechanical and barrier properties differently across formulations. While PVA/XGL1 achieved the best overall balance between strength, flexibility, and reduced permeability, other formulations also presented specific advantages, such as increased tensile strength in PVA/$H_2O$. These results highlight that the hydrophilic nature of both PVA and XG requires careful optimization of blend composition to achieve balanced properties.

### 3.2.7. Water contact angle and water vapor permeability

The water contact angle and wettability values for pure PVA and polymer blend films are presented in **Table 6**. Pure PVA and PVA/$H_2O$ films exhibited the lowest contact angles, measuring 64.96° and 58.17°, respectively. A possible explanation for this behavior lies in the chemical structure of PVA. The presence of numerous hydroxyl groups along the polymer chains promotes strong interactions with water molecules through hydrogen bonding, which contributes to its pronounced hydrophilic character [38].

**Table 6.** Contact angle, wettability, and water vapor permeability of PVA and polymer blend films.

| Film | Contact angle (°) | Wettability | WVP ((g·m·m)/m²·h·KPa) | WVTR (g/m²·day) |
|---|---|---|---|---|
| PVA | 64.96 ± 0.67 [b] | 0.05 ± 0.01 [b] | 0.882 ± 0.143 [d] | 12.199 ± 1.690 [d] |
| PVA/$H_2O$ | 58.17 ± 2.60 [a] | 0.03 ± 0.03 [a] | 0.333 ± 0.143 [c] | 10.366 ± 3.200 [c] |
| PVA/XG | 75.78 ± 1.47 [d] | 0.03 ± 0.03 [a] | 0.289 ± 0.143 [b] | 7.385 ± 2.459 [b] |
| PVA/XGL1 | 80.81 ± 2.20 [e] | 0.03 ± 0.02 [a] | 0.243 ± 0.143 [a] | 5.257 ± 0.851 [a] |
| PVA/XGL2 | 74.43 ± 2.12 [c] | 0.03 ± 0.01 [a] | * | * |

For a given column, means followed by the same letter are not significantly different, whereas means followed by different letters differ significantly at the 5% significance level. * Data not available due to experimental instability and mass loss during testing. PVA: polyvinyl alcohol; XG: xanthan gum; XGL1, XGL2: sugarcane bagasse-derived xanthan gum variants; WVP: water vapor permeability; WVTR: water vapor transmission rate.

In contrast, the incorporation of xanthan gum, both commercial and laboratory-produced, led to an increase in water contact angle (approximately 75°), indicating a reduction in surface hydrophilicity. This change may be attributed to the decreased availability of free hydroxyl groups, resulting from intermolecular interactions between PVA and xanthan gum. These interactions, likely involving hydrogen bonding or electrostatic forces, reduce the number of hydroxyl sites accessible for bonding with water molecules, thereby reducing the wettability of the film surface.

Water contact angles below 90° are associated with high wettability and are therefore indicative of hydrophilic surfaces, whereas angles above 90° reflect low wettability, typical of hydrophobic materials [30]. Although the addition of xanthan gum led to a slight increase in contact angle, due to its molecular characteristics, all film samples in this study exhibited values below 90°, confirming their overall hydrophilic nature.

Similarly, in a related study, Patil et al. [30] found a water contact angle value of 55.4°, and a reduction in hydrophilicity (higher contact angles) was correlated with higher PVA content in PVA/starch polymer blends.

The results of water vapor permeability are presented in **Table 6**. From a packaging perspective, controlling water vapor transfer is important because it directly affects the preservation and quality of food products during storage [9]. The addition of xanthan gum modified the barrier behavior of the films, leading to WVP values that differed significantly from those of pure PVA ($p < 0.05$). This trend is consistent with previous reports showing that the incorporation of other polymers can alter the permeability characteristics of PVA-based materials. Pure PVA film presented the highest WVP values, 0.882 ((g·m·m)/m²·h·KPa), which can be attributed to its hydrophilic nature and low water resistance. These characteristics are associated with a high density of hydroxyl groups, leading to increased water affinity, greater film thickness, elevated moisture content, and consequently, enhanced water vapor transmission.

In contrast, the addition of xanthan gum, both commercial and laboratory-produced, into PVA matrix resulted in a marked reduction in WVP and TWVP values, 0.289 and 0.243 ((g·m·m)/m²·h·KPa), and 7.385 and 5.257 (g/m²·day), respectively. These results indicate improved humidity barrier properties, due to the molecular compatibility and interactions between PVA and XG within the film matrix. The formation of strong hydrogen bonds between the polymer chains, particularly in formulations derived from sugarcane bagasse, leads to a more ordered and

cohesive structure. This reduces the presence of voids and microchannels, limiting the diffusion and adsorption of water molecules and contributing to a denser, more compact film structure [9].

It was not possible to obtain WVTR and WVP values for the PVA/XGL2 sample due to irregular mass variations observed in experimental period, which compromised the accuracy of the gravimetric method. As this behavior was not detected in the other formulations, no values are reported for PVA/XGL2. Therefore, no values are reported for this formulation in **Table 6**.

Similar results were reported by [9], who observed that pure PVA films exhibited the highest water vapor permeability values. However, the incorporation of XG into the composite films led to improved barrier properties, resulting in reduced WVP values.

### 3.2.8. FEG-SEM

FEG-SEM images of the surface and cross-sectional morphology of pure PVA and PVA/XG blend films are shown in **Figure 12**. The surface of pure PVA film (**Figure 12a**) appeared homogeneous, smooth, and flat, with no evidence of particle agglomeration, cracks, fissures, or visible pores. The addition of XG (**Figure 12e,g,i**) did not significantly alter the surface morphology, as the blend films also exhibited a compact and uniform structure. The cross-section analysis revealed continuous and homogeneous internal structures (**Figure 12b,d,f,h,j**), without evidence of voids, agglomerates, or phase separation. These morphological characteristics suggest morphological compatibility between PVA and XG. When combined with FTIR results and barrier property analyses, these findings support the interference of good miscibility between the polymers.

The incorporation of xanthan gum appears to enhance the interaction between the blend components by promoting molecular associations with the PVA chains. These interactions, which involve hydrogen bonding and possibly electrostatic forces, favor the development of a more cohesive polymer network and may contribute to the improved stability and compatibility observed in the films [9].

Chen et al. [9] reported similar surface and cross-sectional morphologies for both pure PVA and PVA/XG blend films, highlighting the formation of hydrogen bonds between polymers. These interactions are attributed to the active functional groups of xanthan gum, which can replace water-binding sites and establish intermolecular connections with PVA chains. However, at higher XG concentrations, the surface morphology tends to become more irregular and rough, with the appearance of voids. This behavior was not observed in the present study, as the films maintained a homogeneous structure without signs of heterogeneity.

Similarly, Eelager et al. [13] found that hydrogels with lower XG content and higher PVA content exhibited smooth, uniform, and continuous surfaces, indicating good dispersion and compatibility between polymers. In contrast, increasing the concentration of the biopolymer led to rougher surfaces and the formation of voids, which were associated with the development of an interpenetrating polymer network between PVA and XG.

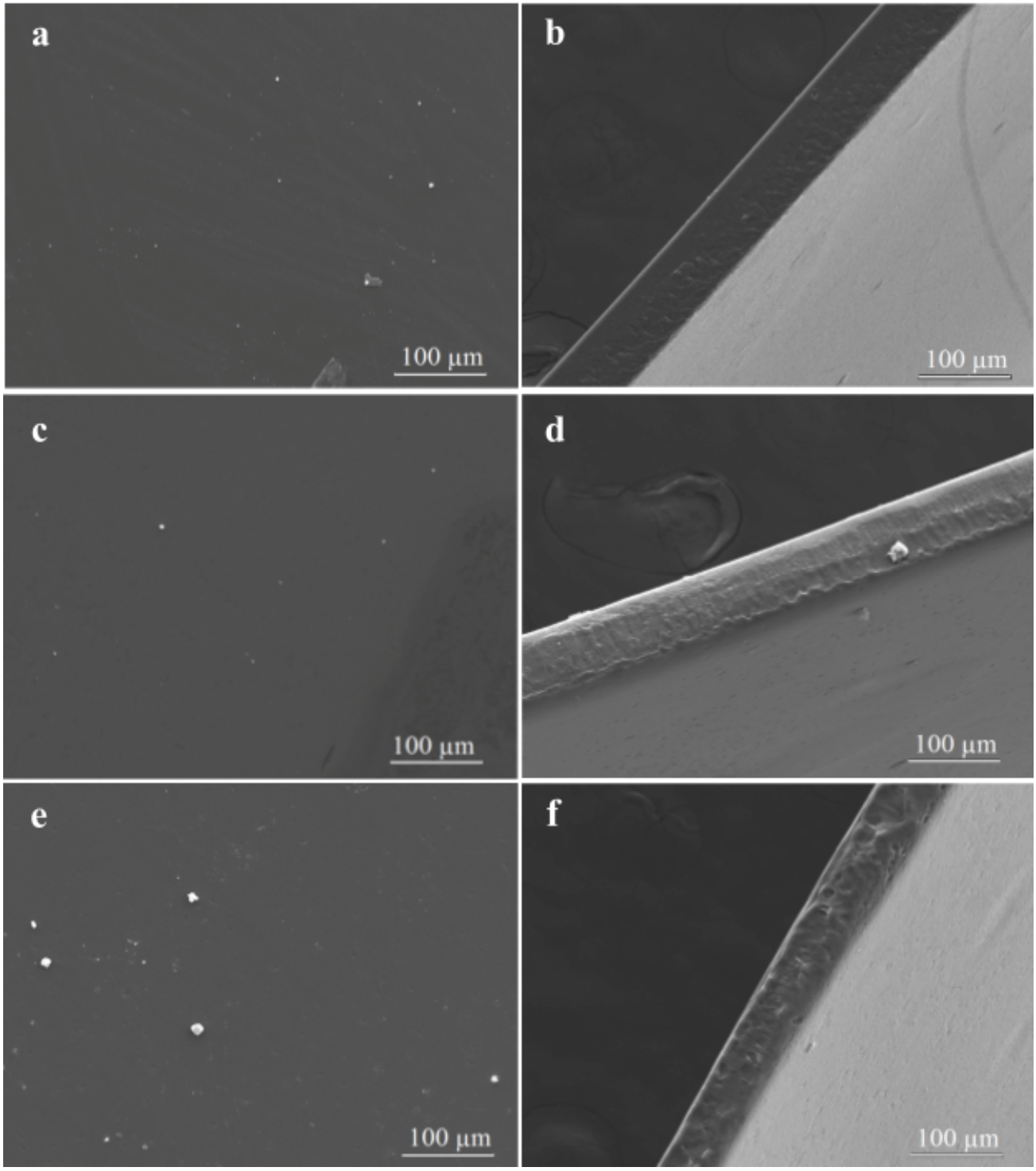



**Figure 12.** *Cont.*

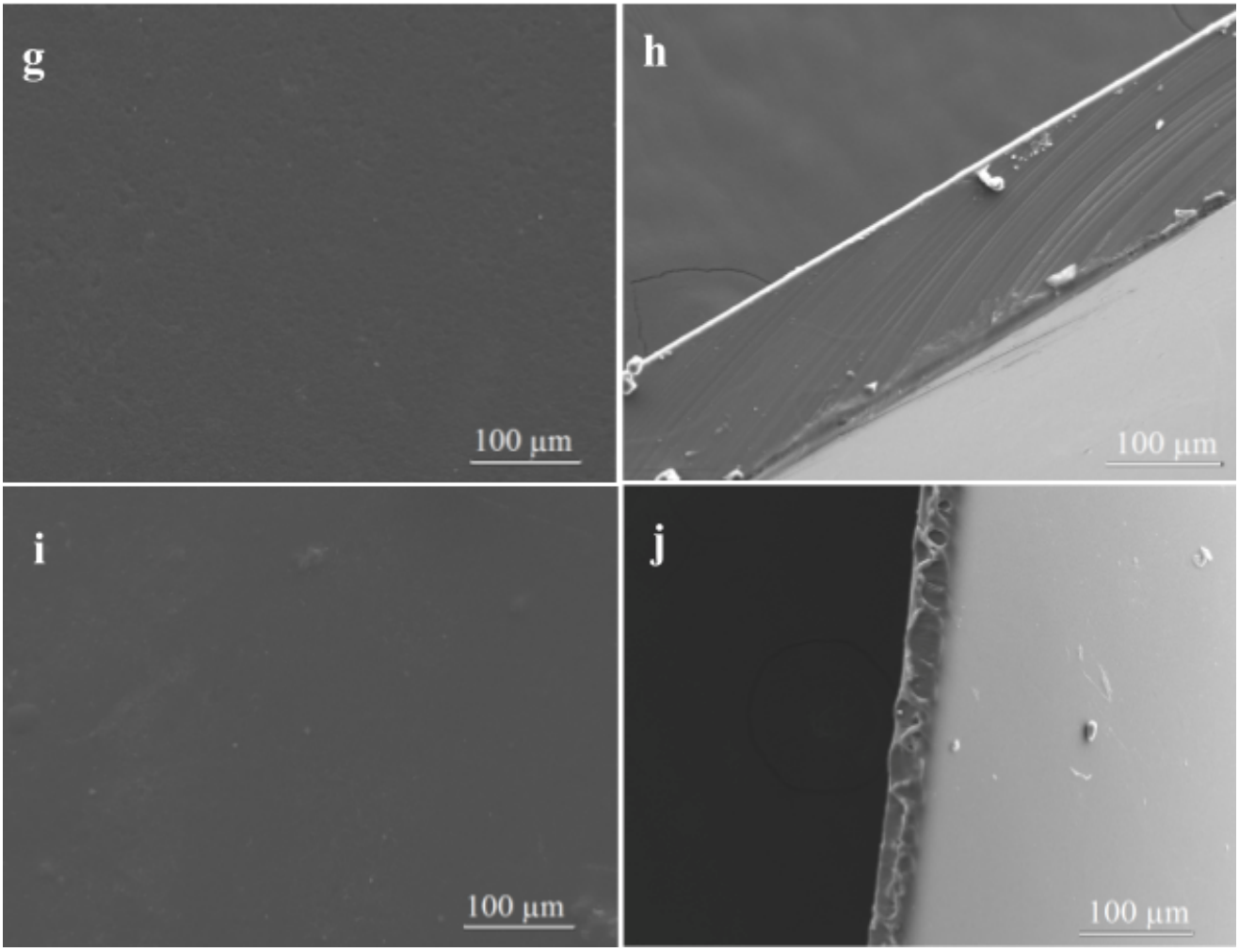



**Figure 12.** Surface and cross-sectional morphology of films: pure PVA (**a**,**b**); PVA/$H_2O$ (**c**,**d**); PVA/XG (**e**,**f**); PVA/XGL1 (**g**,**h**); and PVA/XGL2 (**i**,**j**). Images obtained by FEG-SEM at 500× magnification, operated at 20 kV. PVA: polyvinyl alcohol; XG: xanthan gum; XGL1, XGL2: sugarcane bagasse-derived xanthan gum variants; FEG-SEM: Field emission gun scanning electron microscopy.

## 4. Conclusions

The incorporation of xanthan gum, both commercial and laboratory-produced from sugarcane bagasse, into PVA matrices resulted in films with enhanced structural and functional properties. Pure PVA exhibited an average thickness of 0.125 mm and a thermal mass loss of ~58%, while PVA/XG blends showed reduced thickness (0.059–0.064 mm) and lower mass loss (~30%). FTIR suggested intermolecular hydrogen bonding, and SEM revealed continuous and homogeneous morphologies, supporting polymer miscibility.

Among the formulations, PVA/XGL1 demonstrated the ideal performance, with tensile strength of 34 MPa and elongation at break of 270.97%, lowest water vapor permeability (0.243 g·mm/$m^2$·h·kPa), and highest contact angle (80.81°), evidencing improved barrier properties and mechanical robustness.

Producing xanthan gum from sugarcane bagasse adds environmental value, aligning with SDG 9, SDG 12, and SDG 13. By converting agro-industrial residues into high-value biopolymers and integrating them into biodegradable matrices, this study offers a viable and sustainable alternative to fossil-based plastics.

Overall, PVA/XGL1 stands out as a promising formulation, combining mechanical strength, controlled thermal degradation, and superior barrier properties, while promoting residue valorization. Future work should investigate biodegradation behavior and practical applications such as fruit packaging, particularly strawberries.

## Acknowledgments

The authors extend their sincere thanks to the Laboratory of Electron Microscopy and Analysis of Ultrastructural Federal University of Lavras, and to Packaging Technology Center (CETEA)/Institute of Food Technology (ITAL), Campinas, Brazil for conducting specific analyses. Appreciation is further expressed to the academic institutions Federal University of Lavras (UFLA), University of Copenhagen (KU), and the Federal University of São João del-Rei (UFSJ) for their collaboration and support, and Minas Gerais State Research Support Foundation (FAPEMIG) and Funding Authority for Studies and Projects (FINEP) for their support throughout the project. The authors acknowledge the use of the AI tool Microsoft Copilot for language editing. The tool was applied to enhance clarity and scholarly tone, and all edits were carefully reviewed and validated by the authors to ensure accuracy, compliance with academic standards, and research integrity. The authors fully support Academia.edu Journals' adherence to COPE guidelines on AI in publication ethics and confirm that this use has been managed responsibly and ethically.

## Funding

This research was sponsored by Coordination for the Improvement of Higher Education Personnel (CAPES) under grant numbers 88887.816195/2023-00 and 88887.618161/2021-00; and by National Council for Scientific and Technological Development (CNPq) under grant number 201015/2022-6.

## Author contributions

Conceptualization, M.R.M.F.d.C., E.N.d.O.J., M.V.D., G.H.D.T. and M.G.J.; methodology, M.R.M.F.d.C., E.N.d.O.J., M.V.D., F.G.T., J.C., L.G.T., A.R.S. and M.G.J.; formal analysis, M.R.M.F.d.C.; resources, G.H.D.T.; data curation, M.R.M.F.d.C., E.N.d.O.J. and L.G.T.; writing—original draft preparation, M.R.M.F.d.C.; writing—review and editing, M.R.M.F.d.C., E.N.d.O.J., M.V.D., F.G.T., J.C., L.G.T., A.R.S. and M.G.J.; supervision, M.G.J.; project administration, M.G.J.; funding acquisition, G.H.D.T. All authors have read and agreed to the published version of the manuscript.

## Conflict of interest

The authors declare that they have no competing interests, and that the funding sponsors played no role in the study's conception, design, execution, or interpretation, or with the writing of this manuscript.

## Data availability statement

All data supporting the findings of this publication are available within this article.

## Publisher's note

Academia.edu Journals stays neutral regarding jurisdictional claims in published maps and institutional affiliations. All claims expressed in this article are solely those of the authors and do not necessarily represent those of their affiliated organizations, or those of the publisher, the editors, and the reviewers. Any product that may be evaluated in this article, or claim that may be made by its manufacturer, is not guaranteed or endorsed by the publisher.

## Copyright

© 2026 copyright by the authors. This article is an open access article distributed under the terms and conditions of the Creative Commons Attribution (CC BY) license.

## References

1. Hadi A, Nawab A, Alam F, Zehra K. Sustainable food packaging films based on alginate and aloe vera. Polym Eng Sci. 2022; 62 (7): 2111–8. doi: 10.1002/pen.25992
2. D'Almeida AP, de Albuquerque TL. Innovations in food packaging: from bio-based materials to smart packaging systems. Processes. 2024; 12 (10): 2085. doi: 10.3390/pr12102085
3. Yin Y, Woo MW. Transitioning of petroleum-based plastic food packaging to sustainable bio-based alternatives. Sustain Food Technol. 2024; 2 (3): 548–66. doi: 10.1039/d4fb00028e
4. Guzman-Puyol S, Benítez JJ, Heredia-Guerrero JA. Transparency of polymeric food packaging materials. Food Res Int. 2022; 161: 111792. doi: 10.1016/j.foodres.2022.111792
5. Tabassum Z, Anand A, Bhanot R, Girdhar M, Kumar A, Mamidi N, et al. Xanthan gum-driven innovations for reinventing food preservation. Polymers. 2025; 17 (23): 3160. doi: 10.3390/polym17233160
6. Shaikh S, Yaqoob M, Aggarwal P. An overview of biodegradable packaging in food industry. Curr Res Food Sci. 2021; 4: 503–20. doi: 10.1016/j.crfs.2021.07.005
7. Chen J, Zheng M, Tan KB, Lin J, Chen M, Zhu Y. Development of xanthan gum/hydroxypropyl methyl cellulose composite films incorporating tea polyphenol and its application on fresh-cut green bell peppers preservation. Int J Biol Macromol. 2022; 211: 198–206. doi: 10.1016/j.ijbiomac.2022.05.043
8. Fan Y, Ren J, Cao Y, Zou Y, Xiao X, Liu F. Recent advances in polyvinyl alcohol–based biodegradable packaging: preparation, modification, and applications in food packaging. Compr Rev Food Sci Food Saf. 2025; 24 (6): e70334. doi: 10.1111/1541-4337.70334
9. Chen J, Zheng M, Tan KB, Lin J, Chen M, Zhu Y. Polyvinyl alcohol/xanthan gum composite film with excellent food packaging, storage and biodegradation capability as potential environmentally-friendly alternative to commercial plastic bag. Int J Biol Macromol. 2022; 212: 402–11. doi: 10.1016/j.ijbiomac.2022.05.119
10. Chen G, Li J, Sun Y, Wang Z, Leeke GA, Moretti C, et al. Replacing traditional plastics with biodegradable plastics: impact on carbon emissions. Engineering. 2024; 32: 152–62. doi: 10.1016/j.eng.2023.10.002
11. Xu Y, Wu Z, Li A, Chen N, Rao J, Zeng Q. Nanocellulose composite films in food packaging materials: a review. Polymers. 2024; 16 (3): 423. doi: 10.3390/polym16030423
12. Utracki LA, editor. Polymer blends handbook. Vol. 1. Dordrecht, The Netherlands: Kluwer Academic Publishers; 2002.

13. Eelager MP, Masti SP, Dalbanjan NP, Madihalli S, Gunaki MN, Kurbetta LK, et al. Atrazine integrated biodegradable poly(vinyl alcohol)/xanthan gum active films for mulching applications: an alternative to microplastic generation plastic mulch. Prog Org Coat. 2024; 192: 108510. doi: 10.1016/j.porgcoat.2024.108510
14. Brunchi CE, Bercea M, Morariu S, Avadanei M. Investigations on the interactions between xanthan gum and poly(vinyl alcohol) in solid state and aqueous solutions. Eur Polym J. 2016; 84: 161–72. doi: 10.1016/j.eurpolymj.2016.09.006
15. da Costa MRMF, de Oliveira Junior EN, Dias MV, Thygesen LG, Tonoli GHD, Sanadi AR, et al. Xanthan gum production from sugarcane bagasse and its potential for biodegradable food packaging films. Food Bioprod Process. 2026; 156: 191–9. doi: 10.1016/j.fbp.2026.01.008
16. Lide DR, editor. CRC handbook of chemistry and physics: a ready-reference book of chemical and physical data. 85th ed. Boca Raton, FL, USA: CRC Press; 2004.
17. O'Brien FE. The control of humidity by saturated salt solutions. J Sci Instrum. 1948; 25 (3): 73–6. doi: 10.1088/0950-7671/25/3/305
18. Vertucci CW, Roos EE. Theoretical basis of protocols for seed storage II. The influence of temperature on optimal moisture levels. Seed Sci Res. 1993; 3 (3): 201–13. doi: 10.1017/S0960258500001793
19. International Organization for Standardization. Plastics—film and sheeting—determination of thickness by mechanical scanning. ISO 4593:1993. Geneva, Switzerland: ISO; 1993.
20. Rodrigues R, Patil S, Dhakane-Lad J, Nadanathangam V, Mahapatra A. Effect of green tea extract, ginger essential oil and nanofibrillated cellulose reinforcements in starch films on the keeping quality of strawberries. J Food Process Preserv. 2022; 46: e16109. doi: 10.1111/jfpp.16109
21. Nunes JC, Melo PTS, Aouada FA, Moura MRD. Influence of lemon nanoemulsion in films gelatin-based. Quim Nova. 2018; 41 (9): 1006–10.
22. Meydanju N, Pirsa S, Farzi J. Biodegradable film based on lemon peel powder containing xanthan gum and $TiO_2$–Ag nanoparticles: investigation of physicochemical and antibacterial properties. Polym Test. 2022; 106: 107445. doi: 10.1016/j.polymertesting.2021.107445
23. Liu F, Jiang L, Yang S. Ultra-violet degradation behavior of polymeric backsheets for photovoltaic modules. Sol Energy. 2014; 108: 88–100. doi: 10.1016/j.solener.2014.06.027
24. Sahora V, Khan H, Raghuvanshi S, Dutt D. Development of polyvinyl alcohol-based antioxidant nanocomposite films with nanokaolin impregnated with polyphenols from pomegranate peel extract. Food Packag Shelf Life. 2022; 32: 100848. doi: 10.1016/j.fpsl.2022.100848
25. Ponzecchi A, Alfredsen G, Fredriksson M, Thybring EE, Thygesen LG. Localization and characterisation of brown rot in two types of acetylated wood. Cellulose. 2024; 31: 1875–90. doi: 10.1007/s10570-023-05680-0
26. ASTM International. Standard test methods for tensile properties of thin plastic sheeting. ASTM D882-18. West Conshohocken, PA, USA: ASTM International; 2018.
27. Al Aita A, Aslam M, Smarandache F. A new mood's median test for imprecise data. Infinite Study. 2024; 22: 95. doi: 10.28924/2291-8639-22-2024-95
28. ASTM International. Standard test methods for water vapor transmission of materials. ASTM E96/E96M-24. West Conshohocken, PA, USA: ASTM International; 2024.
29. Lara BRB, de Andrade PS, Guimaraes Junior M, Dias MV, Alcântara LAP. Novel whey protein isolate/polyvinyl biocomposite for packaging: Improvement of mechanical and water barrier properties by incorporation of nano-silica. J Polym Environ. 2021; 29: 2397–408. doi: 10.1007/s10924-020-02033-x
30. Patil S, Bharimalla AK, Mahapatra A, Dhakane-Lad J, Arputharaj A, Kumar M, et al. Effect of polymer blending on mechanical and barrier properties of starch-polyvinyl alcohol based biodegradable composite films. Food Biosci. 2021; 44 (PtA): 101352. doi: 10.1016/j.fbio.2021.101352

31. Garavand Y, Taheri-Garavand A, Garavand F, Shahbazi F, Khodaei D, Cacciotti I. Starch-polyvinyl alcohol-based films reinforced with chitosan nanoparticles: physical, mechanical, structural, thermal and antimicrobial properties. Appl Sci. 2022; 12 (3): 1111. doi: 10.3390/app12031111
32. Rodrigues NLG, Thielemans W, Dufresne A. Sisal cellulose whiskers reinforced polyvinyl acetate nanocomposites. Cellulose. 2006; 13: 261–70. doi: 10.1007/s10570-005-9039-7
33. Rotta J, Ozório RÁ, Kehrwald AM, de Oliveira Barra GM, Amboni RDDMC, Barreto PLM. Parameters of color, transparency, water solubility, wettability and surface free energy of chitosan/hydroxypropylmethylcellulose (HPMC) films plasticized with sorbitol. Mater Sci Eng C. 2009; 29 (2): 619–23. doi: 10.1016/j.msec.2008.10.032
34. Rico-Rodríguez F, López-Padilla A, Ortega-Toro R. Biodegradable polyvinyl alcohol (PVOH)-based films with anthocyanin-rich extracts of corozo (*Bactris guineensis* H.E. Moore) for intelligent packaging design. Polymers. 2025; 17 (7): 933. doi: 10.3390/polym17070933
35. Bhatia S, Al-Harrasi A, Shah YA, Saif Alrasbi AN, Jawad M, Koca E, et al. Structural, mechanical, barrier and antioxidant properties of pectin and xanthan gum edible films loaded with grapefruit essential oil. Heliyon. 2024; 10 (3): e25501. doi: 10.1016/j.heliyon.2024.e25501
36. Hermawan D, Lai TK, Jafarzadeh S, Gopakumar DA, Owolabi FAT, Aprilia NA, et al. Development of seaweed-based bamboo microcrystalline cellulose films intended for sustainable food packaging applications. BioResources. 2019; 14 (2): 3389–410. doi: 10.15376/biores.14.2.3389-3410
37. Tavassoli M, Bahramian B, Abedi-Firoozjah R, Jafari N, Javdani H, Sadeghi SM, et al. Comprehensive review on polyvinyl alcohol-based electrospun nanofibers for food packaging: applications, developments, and future horizon. Food Bioprocess Technol. 2025; 18: 3223–44. doi: 10.1007/s11947-024-03637-0
38. Abedi-Firoozjah R, Chabook N, Rostami O, Heydari M, Kolahdouz-Nasiri A, Javanmardi F, et al. PVA/starch films: an updated review of their preparation, characterization, and diverse applications in the food industry. Polym Test. 2022; 118: 107903. doi: 10.1016/j.polymertesting.2022.107903
39. Sirbu EE, Dinita A, Tănase M, Portoacă AI, Bondarev A, Enascuta CE, et al. Influence of plasticizers concentration on thermal, mechanical, and physicochemical properties on starch films. Processes. 2024; 12 (9): 2021. doi: 10.3390/pr12092021
40. Wang S, Ren J, Li W, Sun R, Liu S. Properties of polyvinyl alcohol/xylan composite films with citric acid. Carbohydr Polym. 2014; 103: 94–9. doi: 10.1016/j.carbpol.2013.12.030
41. Othornvit R, Krochta JM. Plasticizer effect on oxygen permeability of β-lactoglobulin films. J Agric Food Chem. 2000; 48 (12): 6298–302. doi: 10.1021/jf000836l
42. Gomes GV, Assis DDJ, da Silva JB, Santos-Ebinuma VDC, Costa LA, Druzianl JI. Obtaining xanthan gum impregnated with cellulose microfibrils derived from sugarcane bagasse. Mater Today Proc. 2015; 2 (1): 389–98. doi: 10.1016/j.matpr.2015.04.042
43. Jones H, McClements J, Ray D, Hindle CS, Kalloudis M, Koutsos V. Thermomechanical properties of virgin and recycled polypropylene-high-density polyethylene blends. Polymers. 2023; 15 (21): 4200. doi: 10.3390/polym15214200